

# AeroHaptix: A Wearable Vibrotactile Feedback System for Enhancing Collision Avoidance in UAV Teleoperation

Bingjian Huang, Zhecheng Wang, Qilong Cheng, Siyi Ren, Hanfeng Cai, Antonio Alvarez Valdivia, Karthik Mahadevan, and Daniel Wigdor

**Abstract**—Haptic feedback enhances collision avoidance by providing directional obstacle information to operators in unmanned aerial vehicle (UAV) teleoperation. However, such feedback is often rendered via haptic joysticks, which are unfamiliar to UAV operators and limited to single-directional force feedback. Additionally, the direct coupling of the input device and the feedback method diminishes the operators’ control authority and causes oscillatory movements. To overcome these limitations, we propose AeroHaptix, a wearable haptic feedback system that uses high-resolution vibrations to communicate multiple obstacle directions simultaneously. The vibrotactile actuators’ layout was optimized based on a perceptual study to eliminate perceptual biases and achieve uniform spatial coverage. A novel rendering algorithm, MultiCBF, was adapted from control barrier functions to support multi-directional feedback. System evaluation showed that AeroHaptix effectively reduced collisions in complex environment, and operators reported significantly lower physical workload, improved situational awareness, and increased control authority.

## I. INTRODUCTION

Unmanned aerial vehicle (UAV) teleoperation allows operators to pilot UAVs beyond visual line of sight, enabling the performance of tasks in areas that are either difficult or dangerous for humans to access. However, it is a challenging task because the operator is physically separated from the UAV, which limits operators’ abilities to perceive obstacles and avoid collisions. Novel UAV teleoperation systems have utilized haptic feedback to deliver obstacle information so that operators can safely steer UAVs. To translate obstacle information into haptic feedback, prior work has developed collision avoidance algorithms such as parametric risk fields [1], time-to-impact [2], dynamic kinesthetic boundary [3], and control barrier functions (CBF) [4].

Despite the advancement of collision avoidance algorithms, the devices used to render haptic feedback are primarily commercial haptic joysticks with three degree-of-freedom (DoF) force feedback [5]–[7]. Although these devices have proven useful in collision avoidance tasks [8], [9], they are rarely adopted in real-world UAV operations due to the high cost of transitioning from standard radio control (RC) controllers to these unfamiliar devices. Additionally, their usage is constrained to indoor environments as they require mounting to provide force feedback. Furthermore, their limited information bandwidth restricts force feedback to being rendered in one direction [4], [10], thus compromising situational awareness in environments with multiple obstacles. Since the force feedback is exerted on the hand, the direct coupling of input and output channels impairs UAV

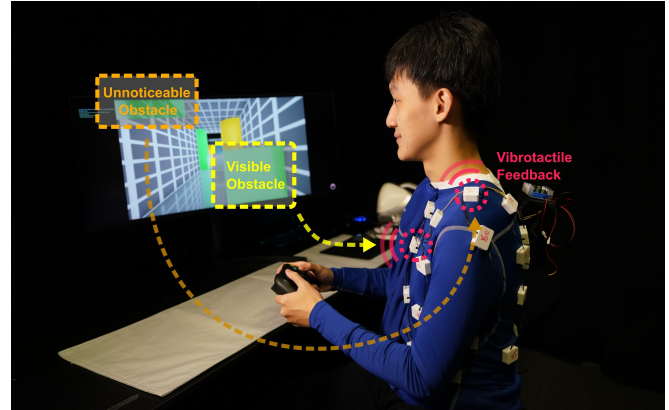


Fig. 1: AeroHaptix assists UAV operators with collision avoidance by delivering obstacle directions via multi-point vibrotactile feedback on the body. Operators not only see and feel visible obstacles (yellow), but also perceive obstacles out of the view (orange).

control precision, leading to oscillatory behavior in cluttered environments [9] and low user acceptance [11].

To address these limitations, we designed a wearable haptic feedback system, AeroHaptix, that uses vibrotactile feedback at thirty-two upper body positions to deliver obstacle directions. Since the feedback is provided as vibration cues on the body, it does not hinder hand movement and can be seamlessly integrated into existing teleoperation control workflows (e.g., using RC controllers). To optimize the layout of vibrotactile actuators on the body, we conducted a perceptual study with ten participants to collect data on the mapping between body positions and spatial directions, and employed a data-driven method to generate the final layout. We also designed MultiCBF, a new collision avoidance algorithm based on previous CBF methods to render multi-directional haptic feedback. To evaluate AeroHaptix’s performance, we conducted a comparative study in a simulated environment, where participants maneuvered a UAV through tunnels with obstacles, assisted by different haptic devices. The results showed that AeroHaptix effectively reduced collisions in complex environment, with significantly lower operator workload, better situational awareness, and increased control authority.

## II. RELATED WORK

Of most relevance to the present research is prior literature on (a) collision avoidance algorithms for UAV teleoperation and (b) vibrotactile feedback to convey spatial information.

### A. Collision Avoidance Algorithms

Collision avoidance algorithms were first utilized for unmanned ground vehicle (UGV) teleoperation. In 1998, Hong et al. [12] proposed an artificial force field (AFF) algorithm to generate artificial forces based on the potential fields of vehicle and obstacles. The concept was later adopted for unmanned aerial vehicles (UAVs) by Boschloo et al. [13] and Lam et al. [1], who developed basic risk field (BRF) and parametric risk field (PRF) algorithms respectively. These methods successfully reduced collisions but faced difficulties in navigating through narrow spaces. To further improve operation, Brandt and Colton [2] introduced time-to-impact (TTI) and virtual string (VS) algorithms, which calculated the virtual impact forces between a UAV and obstacles. While these algorithms further reduced collisions and workloads, the force feedback could cause UAVs to oscillate in cluttered environments [9].

Alternatively, other researchers have proposed algorithms that override user inputs with safer values, such as dynamic kinesthetic boundary (DKB) [3], [14] and obstacle avoidance system for teleoperation (OAST) [15]. While these algorithms eliminated all collisions, they deprived operators of control authority and resulted in low user acceptance. More recently, Zhang et al. [4] applied control barrier functions (CBF) to UAV teleoperation and helped reduce both collisions and workloads. Moreover, they designed a haptic shared autonomy control scheme that enhanced the operators' perceived control authority [8]. Our research built on this by modifying the CBF algorithm to support multi-point haptic feedback by enabling the simultaneous representation of multiple obstacles.

### B. Vibrotactile Feedback to Convey Spatial Information

Vibrotactile feedback leverages the human tactile sense to convey information or create experiences by generating vibrations on the skin. Our objective is to employ vibrotactile feedback to convey obstacle directions during UAV teleoperation. Prior work has demonstrated the application of vibrotactile feedback in various domains where spatial information is crucial. For example, vibrotactile headbands have been used to assist users in locating 3D objects and improving spatial awareness in virtual reality [16], [17]. Vibrotactile actuators have also been mounted on the body to enhance obstacle detection and navigation for blind and visually-impaired people [18]–[20]. Within robotics, vibrations have been used to communicate handover positions and predicted trajectories of robotic arms [21], [22], hydrodynamic flow near underwater robots [23], and obstacle positions around UGVs [24]. These examples reaffirm the applicability of using vibrotactile feedback to convey spatial information.

Compared to previous applications, delivering obstacle directions during UAV teleoperation could be more challenging, because it requires numerous actuators with custom layout on the body to represent obstacle directions precisely. Current vibrotactile systems such as TactJam [25] and VHP [26] offer increased customizability but only support less than 10 actuators. In contrast, solutions like bHaptics X40 [27])

support numerous actuators but have predetermined positions and limited body coverage. Therefore, we developed a custom hardware solution for AeroHaptix which fulfilled the above requirements.

### III. VIBROTACTILE HARDWARE DESIGN

To support haptic UAV teleoperation tasks, AeroHaptix was designed to support numerous actuators, customized layout, and low-latency control. It had the following three requirements:

- **R1**: support a large number of actuators with fine-grained control so that obstacles from different directions could be distinguished;
- **R2**: support reconfigurable layouts so actuator positions could be freely adjusted as needed.
- **R3**: support low-latency communication so multi-point feedback could be activated without noticeable delays;

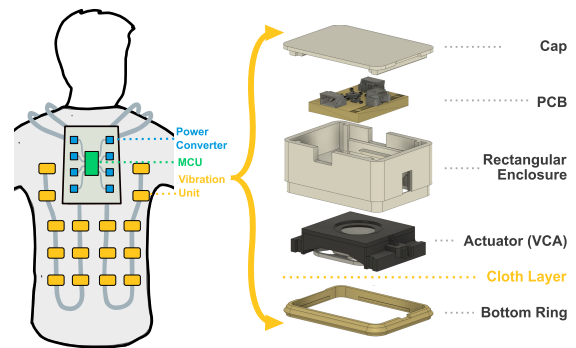


Fig. 2: Hardware design overview and the exploded view of each vibration unit.

AeroHaptix had a central unit and multiple chains of vibration units (Figure 2). Each vibration unit consisted of a vibrotactile actuator, a custom-designed PCB board, and 3D-printed enclosures (Figure 2). A voice coil actuator (VCA) was used as the actuator (PUI Audio, Model# = HD-VA3222). It was 32 mm by 22 mm, with wide-range frequency responses from 80 - 500 Hz. When driven by 133 Hz 1.5  $V_{rms}$  signal, it had a maximum acceleration of 2.52 Gp-p. The PCB included a PIC16F18313 Microcontroller Unit (MCU) and a DRV8837 H-bridge motor driver. The MCU received and transmitted UART commands and generated waveforms. When the MCU received a *start* signal, it sent a waveform to the H-bridge to activate the actuator. The MCU had fine-grained control (**R1**) over 16 intensity levels, 4 frequencies, and two waveforms. The 3D-printed enclosure consisted of three parts: the cap and the enclosure ensured components' stability during vibrations, while the bottom ring enabled easy repositioning (**R2**) by attaching the unit to fabric via press-fit.

To support low-latency communication (**R3**), we designed a chain-connection topology and a high-speed UART protocol (Figure 3). Each chain had a central controller, a power converter, and a maximum of 20 vibration units. Each vibration unit received a UART command from the previous unit and determined whether to execute it or propagate it

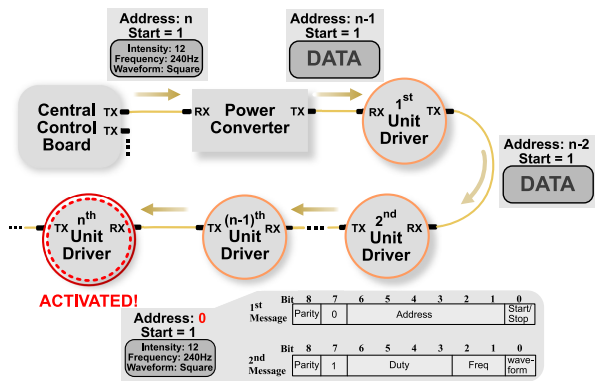


Fig. 3: Data transmission on the chain with two-byte UART protocol. The central unit sends a command with address  $n$ , and each unit deduces the address by 1 until it reaches the target unit.

to the next unit. The UART protocol transmitted two-byte messages at a baud rate of 115.2 kHz with parity check bits. The first byte contained the target unit address, and a *start/stop* toggle bit. The second byte contained vibration parameters for the target unit, including intensity, frequency, and waveform.

A technical evaluation using an oscilloscope concluded that the transmission delay between two vibration units averaged 125  $\mu$ s. For a configuration with 20 units on a chain, the total delay was approximately 2.5 ms, resulting in a 400 Hz refresh rate and real-time control of multiple actuators with imperceptible delay (**R3**).

#### IV. HAPTIC ACTUATOR LAYOUT OPTIMIZATION

To achieve comprehensive coverage of obstacle directions (**R1**), one naive approach would be uniformly distributing actuators around the body. However, previous research has shown that due to proprioceptive biases, a uniform actuator layout on the waist led to uneven coverage of 2D directions in the azimuth plane [28]. Therefore, we designed a perceptual study to collect data on position-direction mappings on the upper body. Then we used machine learning methods to remove biases and produce the optimized actuator layout.

Ten participants (6 male, 4 female; mean age = 25 years, std = 2 years) were recruited for the study. Teleoperation experience was not a requirement for participation. Each experiment lasted 40 minutes and each participant received \$20 CAD as compensation. The study was approved by the university research ethics board.

##### A. Data Collection Procedure

We conducted the study using a 46-actuator grid uniformly distributed on the upper body (shown as red dots in Figure 5). Each actuator was positioned equidistantly from its neighbors, with 18 actuators on the front and back, 3 on each side of the waist, and 2 on each shoulder. Following VibroMap [29], the inter-actuator distances were about 8 cm.

A Unity 3D virtual reality application was developed for the study. Participants wore a Meta Quest 2 headset and stood in a virtual space with coordinates (Figure 4). They received a vibrotactile cue from individual actuators and



Fig. 4: Left: an illustration of the virtual reality study environment. The user points to a spatial direction when perceiving a vibration on the body. Right: sample data points collected from one participant. Points of the same color are from the same actuator.

interpreted it as a directional cue. Then they used the Quest 2 controller with extended ray to pointed to the perceived direction and clicked the trigger button to confirm the choice. Each participant completed 230 trials in a randomized order (i.e., 46 actuators x 5 repetitions).

##### B. Layout Optimization

We collected 2,300 mappings between an actuator’s position on the body surface  $p \in \Omega \subset \mathbb{R}^3$  and the perceived obstacle direction  $(\vartheta, \varphi)$  on a 2-sphere  $S^2$ , parameterized by a polar angle  $\vartheta$  and an azimuth angle  $\varphi$ . This data was used to approximate an inverse mapping from  $S^2$  to  $\Omega \subset \mathbb{R}^3$  using a Multi-layer Perceptron neural network

$$f_\theta = \arg \min_{\theta} \sum_{i=1}^N \|f_\theta(\vartheta, \varphi) - p\|^2 + \lambda \sum_{i=1}^N |\nabla f_\theta(\vartheta, \varphi)|, \quad (1)$$

where  $\theta$  represented the neural network parameters, and  $\lambda$  was the regularization term weight. The network featured five 64-unit hidden layers with ReLU activation. To promote mapping smoothness, we incorporated a total variation regularization term into the mean squared error loss function.

##### C. Final Layout

Previous studies have revealed that humans can discriminate force feedback directions on the hand with 30° resolutions [30], [31]. To achieve similar discriminability with vibrations on the body, we uniformly sampled 32 directions  $\phi = (\vartheta, \varphi)$  in 3D space  $S^2$ , where  $\vartheta \in \{\frac{\pi}{6}, \frac{\pi}{3}, \frac{\pi}{2}, \frac{2\pi}{3}\}$  and  $\varphi \in \{-\frac{3\pi}{4}, -\frac{\pi}{2}, -\frac{\pi}{4}, 0, \frac{\pi}{4}, \frac{\pi}{2}, \frac{3\pi}{4}, \pi\}$ . We then used  $f_\theta$  to find the corresponding actuator positions (blue dots in Figure 5). The final layout indicated that actuators should be positioned on body surface with greater curvatures (e.g., shoulders, waist) for optimal coverage of obstacle directions (**R1**). Directions with  $\vartheta = \frac{5\pi}{6}$  were omitted from the final layout because they did not align with upper body vibrations perceived by users.

In our collision avoidance algorithm MultiCBF, this optimized layout was represented by a set of 32 actuators  $\mathcal{A} = \{\mathcal{A}_i\}_{i=1}^{32}$  and the corresponding directions set  $\hat{r}$  where  $\hat{r}_i$  represents the direction associated with actuator  $\mathcal{A}_i$ .



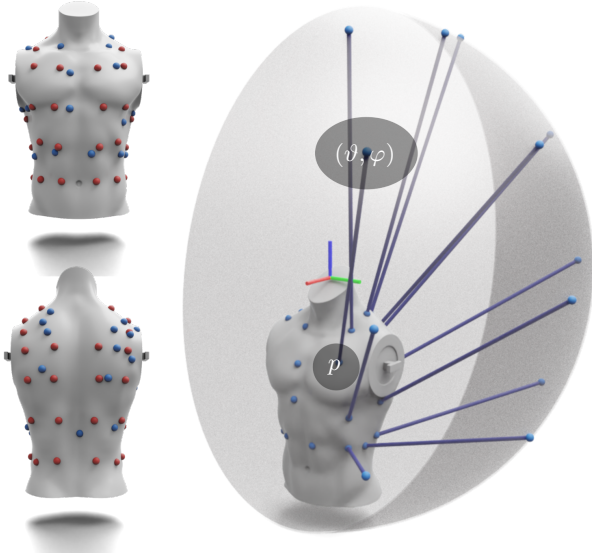


Fig. 5: The vibrotactile actuator layout. The red dots depict the initial uniform distribution used in the perception study, whereas the blue dots depict the final optimized layout. The lines illustrate the connections between spatial directions and body positions on the left side of the body.

## V. COLLISION AVOIDANCE ALGORITHM

In prior work, collision avoidance algorithms such as PRF [32] and CBF [4] only considered single-directional feedback due to the limitations of haptic joysticks. Since AeroHaptix supported multi-point vibrations (**R2**), we extended CBF [4] and built our customized multi-directional feedback algorithm, **MultiCBF**:

- 1) Consider that the continuous-time dynamics of a UAV can be modelled with a double integrator, where the control input  $u$  corresponds to the acceleration command of the UAV. Let  $x = [q \ \dot{q}]^T$  with  $q$  and  $\dot{q}$  being the position and the velocity of the UAV respectively. The dynamics of the system then become

$$\dot{x} = \begin{bmatrix} \dot{q} \\ \ddot{q} \end{bmatrix} = f(x) + g(x)u, \quad (2)$$

where  $x \in \mathcal{X} \subset \mathbb{R}^n$ ,  $u \in \mathcal{U} \subset \mathbb{R}^m$ ,  $f : \mathcal{X} \rightarrow \mathbb{R}^n$  and  $g : \mathcal{X} \rightarrow \mathbb{R}^{n \times m}$  are Lipschitz continuous functions.

- 2) Consider a space with a set of obstacles  $\mathcal{B} = \{b_i\}_{i=1}^{|\mathcal{B}|}$ , where every obstacle  $b_i$  is associated with the center of mass  $q_{b_i}$ . For each obstacle  $b_i$ , we construct a set of safety constraints  $\mathcal{C}_i \in \mathcal{X}$  defined as

$$\mathcal{C}_i := \{x \in \mathcal{X} : h_i(x) \geq 0\}, \quad (3)$$

where  $h_i : \mathcal{X} \rightarrow \mathbb{R}$  is a continuously differentiable function that defines the safety boundary of obstacle  $b_i$ ,  $h_i(x) = 0 \Leftrightarrow x \in \partial\mathcal{C}_i$ .

- 3) We define the CBF  $\mathcal{U}_{\text{CBF}}$  for second-order systems as the set of all control inputs that keep the systems in the safe set  $\mathcal{C}$ . For the CBF associated with  $\mathcal{C}_i$

$$\mathcal{U}_{\text{CBF},i}(h_i(x)) = \{u \in \mathcal{U} : L_f^2 h_i(x) + L_g L_f h_i(x)u + K[h_i(x) \ L_f h_i(x)]^T \} \geq 0, \quad (4)$$

where  $L_f h_i(x) = \nabla h_i(x)^T f(x)$ ,  $L_g h_i(x) = \nabla h_i(x)^T g(x)$  are the Lie derivatives of  $h_i(x)$ ,  $L_f^2 h_i(x)$  is the second-order Lie derivative of  $h_i(x)$ , and  $K$  is a positive constant that adjusts the safety margin.

- 4) Given user input  $u_{\text{ref}} \in \mathcal{U}$ , the optimization of a safe input  $u_{\text{safe},i}$  for obstacle  $b_i$  and its  $h_i(x)$  can be formulated as a quadratic program to find a **local safe input**  $u_{\text{safe},i} \in \mathcal{U}_{\text{CBF},i}$  (Eq. 4) that is closest to  $u_{\text{ref}}$

$$u_{\text{safe},i} = \arg \min_{u \in \mathcal{U}} \frac{1}{2} \|u - u_{\text{ref}}\|^2 \text{ s.t. } u \in \mathcal{U}_{\text{CBF},i}(h_i(x)). \quad (5)$$

If  $u_{\text{safe},i} \neq u_{\text{ref}}$ , it means the user input  $u_{\text{ref}}$  violates the safety constraint  $\mathcal{C}_i$ , then an actuator  $\mathcal{A}_j$  is triggered to notify the user. The choice of actuator  $\mathcal{A}_j$  is determined by the most aligned actuator direction  $\hat{r}_k$

$$j = \arg \max_{k \in 1:32} \left( \frac{q_{b_i} - q}{\|q_{b_i} - q\|} \cdot \hat{r}_k \right). \quad (6)$$

The vibration intensity  $I_j$  of actuator  $\mathcal{A}_j$  is then determined by the difference between the user input  $u_{\text{ref}}$  and the safe input  $u_{\text{safe},i}$  multiplied with a gain factor  $K_v$

$$I_j = \|K_v(u_{\text{safe},i} - u_{\text{ref}})\|_2. \quad (7)$$

Our algorithm differs from previous CBFs [4] because they only considered a **global safe input**  $u_{\text{safe}}$  computed from a global safety set  $h(x) = \{h_i(x)\}_{i=1}^{|\mathcal{B}|}$ . While the global safe input helped operators avoid obstacles, it hinders operator's situational awareness when multiple objects were present. In contrast, our algorithm computed local safe input for each obstacle, and rendered haptic feedback independently.

## VI. SYSTEM EVALUATION

To evaluate whether AeroHaptix enhances collision avoidance, situational awareness, and control authority during UAV teleoperation, we designed a comparative study in which participants maneuver a simulated UAV through a complex environment.

Twelve participants were recruited from university campus to participate in the study (11 male, 1 female; mean age = 24 years, std = 3 years). Seven participants had previous experience operating commercial and custom-made quadrotors. Each experiment lasted 70 minutes and each participant received \$40 CAD as compensation. The study was approved by the university research ethics board.

### A. Experimental Conditions

Participants experienced three **feedback conditions**: no feedback (**NA**), force shared control (**FSC**), and vibrotactile shared control (**VSC**). For the NA and VSC conditions, participants used an Xbox controller for input, which had a similar control mechanism as an RC controller. The output device was AeroHaptix with vibrotactile feedback rendered using MultiCBF. For the FSC condition, a Novint Falcon haptic joystick [5] was used for both input and output, similar to previous studies [33], [34]. Force feedback was rendered using previous CBF methods [4].

Condition	Input Device	Feedback Method
NA	RC controller	No feedback
FSC	Haptic joystick	Force feedback
VSC	RC controller	Vibrotactile feedback

Because previous studies often involved complex experimental setups with varying visual capacity [3], [9], [15], it was unclear when haptic feedback was beneficial. In our study, we isolated flying directions to assess how visual capacity influenced haptic feedback reliance. For each **feedback condition**, three **flying directions** (i.e., forward, right, upward) were evaluated to determine the effects of haptic feedback under varying visual information capacity. In the forward direction, operators received substantial visual information on incoming obstacles because the UAV was oriented to face the flying direction. However, in other directions, the UAV’s camera had limited visibility of obstacles, so we hypothesized that this would potentially increase dependence on haptic feedback for collision avoidance.

Based on these conditions and directions, our hypotheses were that compared to NA and VSC,

- (H<sub>1</sub>) VSC would improve collision avoidance,
- (H<sub>2</sub>) VSC would be more effective when visual capacity is limited,
- (H<sub>3</sub>) VSC would reduce task workloads,
- (H<sub>4</sub>) VSC would increase operators’ control authority, and
- (H<sub>5</sub>) VSC would increase situational awareness.

### B. Experimental Setup

The study was performed in a simulated UAV environment built using Microsoft AirSim [35]. During the study, participants operated a simulated quadrotor with a front-facing camera. The simulation was run on an Alienware M15 Laptop with RTX 3060 Ti GPU.

The experimental scene was a  $5 \times 5 \times 50$ m tunnel (Figure 6) that could face forward, right, or upward for different flying directions. The scene contained four planes and fifteen objects that represented three types of obstacles, i.e., cubes, spheres, and cylinders. The safety boundary of plane  $b_i$  was defined as:  $h_i(x) = h_i([q \ \dot{q}]^T) = (q - q_{b_i}) \times \hat{n}_{b_i}$ , where  $q_{b_i}$  was the center of mass and  $\hat{n}_{b_i}$  was the unit normal of plane  $b_i$ . The safety boundary of other obstacles were approximated using super-ellipsoids  $h_i(x) = h([q \ \dot{q}]^T) = (\frac{q_1 - q_{b_i,1}}{a_1})^n + (\frac{q_2 - q_{b_i,2}}{a_2})^n + (\frac{q_3 - q_{b_i,3}}{a_3})^n$ , where  $q_{b_i}$  was the center of mass and  $a$  was the scaling vector of obstacle  $b_i$ . Obstacle positions were randomized to avoid learning effects.

In each simulation frame, the system detected input commands from the controller, received UAV state updates from AirSim, and checked if safety constraints were violated using MultiCBF. If haptic feedback was enabled, then the system would send vibration or force feedback commands to the corresponding output device. At the end of each frame, the system sent the updated UAV state back to AirSim.

At the beginning of the study, the participant reviewed and signed a consent form. Then, the participant was briefed on the study purpose and overall procedure (Figure 1). Following this, the participant experienced three conditions in a

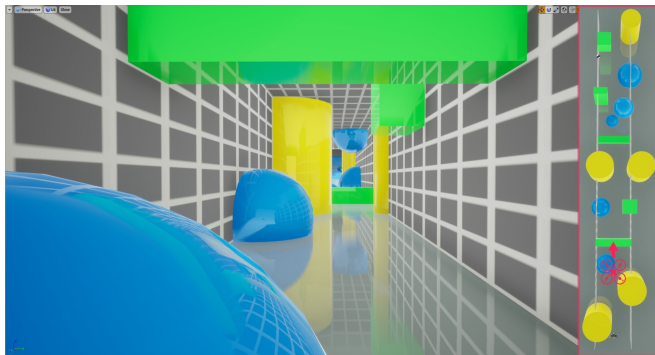


Fig. 6: First-person view of the simulation environment used in the study, with randomly positioned obstacles. A top-down overview is provided on the right.

randomized order ( $3 \times 3$  Latin square). For each condition, the participant underwent a practice round with designated devices for five minutes. Then, the participant operated the UAV to fly through three tunnels, one for each flying direction. After each condition, the participant completed a questionnaire on task workload and control authority.

### C. Metrics and Analysis

We collected both objective and subjective measurements. Objective measurements included the total distance travelled, number of collisions, and input disagreement (computed as the difference between participant input and safe input), which evaluated teleoperation performance and visual capacity effect (**H1**, **H2**). Subjective measurements included NASA-TLX [36] questions that evaluated task load (**H3**), and four 7-point Likert questions adapted from previous work [8] that probed control authority (**H4**), i.e., how easy it was to control the UAV, how much control participants felt over the UAV, how well the UAV matched one’s intentions, and how much the haptic feedback helped UAV navigation.

For each metric, we conducted a two-way repeated measures within-subject ANOVA using SPSS. If the sphericity assumption was violated, the Greenhouse-Geisser correction was used. If the results were significant, i.e., feedback conditions or flying directions had a significant effect, post-hoc pairwise comparisons using a Bonferroni correction were then performed.

To evaluate situational awareness (**H5**), a pop-up window appeared at a random time during the task (with the simulation paused) and participants were prompted to report any perceived obstacles. This design was inspired by situational awareness probing techniques like SAGAT and SPAM [37]. Reported obstacles were categorized into *visual obstacles* that were visible at pause, and *haptic obstacles* that were not seen but perceived through haptic feedback.

### D. Results

1) *Objective Measurements*: For total distance, it was significantly longer when flying right with FSC, and slightly longer when flying right and upward with VSC. The RM-ANOVA determined that feedback condition had a significant effect ( $F(2, 22) = 3.585, p < 0.05$ ), along with flying

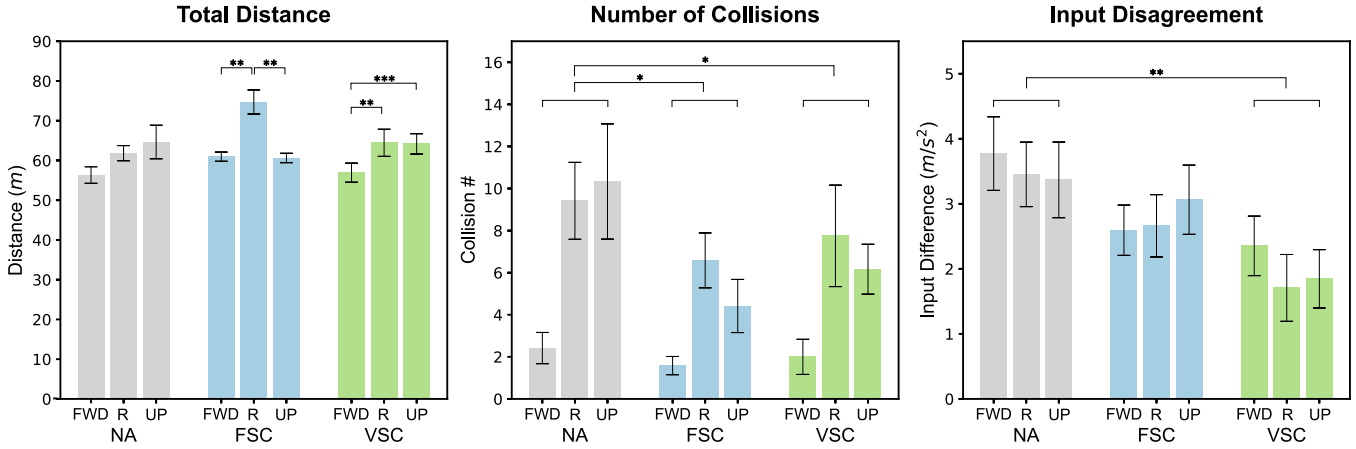


Fig. 7: Objective measurement results grouped by feedback conditions (NA, FSC, VSC) and flying directions (forward, right, upward). The error bars represent the standard error of the mean (SEM), \* $p < 0.05$ , \*\* $p < 0.01$ , and \*\*\* $p < 0.001$ .

direction ( $F(2, 22) = 17.868, p < 0.001$ ). The interaction between feedback condition and flying direction was significant ( $F(1.957, 21.527) = 4.916, p < 0.01$ ). Post-hoc analysis of the interaction effect is shown in Figure 7.

For number of collisions, VSC was significantly lower than NA and comparable to FSC (Figure 7). Right and upward caused more collisions than forward across all conditions. The RM-ANOVA determined that feedback condition had a significant effect ( $F(2, 22) = 8.095, p < 0.01$ ) along with flying direction ( $F(2, 22) = 15.653, p < 0.001$ ). The interaction between feedback condition and flying direction was not significant ( $F(2.168, 23.846) = 1.910, p = 0.168$ ). The post-hoc analysis of feedback conditions revealed that there were significant differences between NA and FSC, NA and VSC, but not FSC and VSC. The post-hoc analysis of flying direction revealed that there were significant differences between forward and right, forward and upward, but not right and upward.

For input disagreement, VSC was significantly smaller than NA (Figure 7). The RM-ANOVA determined that feedback condition had a significant effect ( $F(2, 22) = 4.798, p < 0.05$ ), while flying direction did not ( $F(1.254, 13.789) = 0.628, p = 0.476$ ). The interaction between feedback condition and flying direction was not significant ( $F(4, 44) = 1.566, p = 0.200$ ). The post-hoc analysis of the feedback condition revealed that there were only significant differences between NA and VSC.

In summary, VSC (a) had similar total distances to other conditions, (b) caused fewer collisions than NA, and was comparable to FSC, and (c) reduced input disagreement, helping participants more actively adjust input commands to stay in safe ranges. Thus, **H1** was accepted. Additionally, VSC was more effective on collision avoidance in right and upward directions, highlighting the reliance on haptic feedback under limited visual capacity. Thus, **H2** was accepted.

2) *Subjective Measurements*: The NASA-TLX scores showed that FSC was perceived to be more physically demanding than NA and VSC (Figure 8). In addition, effort and frustration were also higher for FSC, indicating that force feedback induced higher workload for participants.

This could be explained by the responses to the control authority questions (Figure 8), which showed that participants felt they had more control over the UAV when using the Xbox controller (i.e., NA and VSC) than the haptic joystick (i.e., FSC). In addition, they also reported that the UAV movements were more aligned with their intentions when using vibrotactile feedback to steer the UAV. We thus concluded that **H3** and **H4** were accepted.

3) *Situational Awareness*: Regarding flying directions, almost twice as many obstacles were reported moving forward than to the right and upward, due to varying visual capacity (Figure 8). However, with vibrotactile feedback (VSC), participants perceived more obstacles in the latter directions, exceeding the numbers in NA and FSC. Thus, we concluded that VSC enhanced situational awareness, especially when visual capacity was limited. **H5** was accepted.

## VII. DISCUSSION

The results suggested that AeroHaptix significantly enhanced collision avoidance, with reduced workloads, enhanced control authority, and improved situational awareness. In this section, we discuss implications from the results.

### A. Intuitive Mappings from Layout Optimization

The layout optimization process eliminated perceptual biases and ensured an optimal layout on the body, enhancing intuitive mappings between body positions and obstacle directions, which helped reduce workload during teleoperation. This underscored the significance of accounting for perceptual biases in designing haptic feedback systems. Previous approaches that rendered force feedback often overlooked the anisotropy of force perception and magnitude on the hand [30], [31], leading to perceptual differences in force feedback from various directions. This suggested the necessity of addressing perceptual biases in haptic feedback device design before applying to UAV teleoperation.

### B. Effect of Flying Direction and Visual Capacity

The isolation of flying directions helped us assess how visual capacity influenced haptic feedback reliance. The results showed that haptic feedback was less essential for

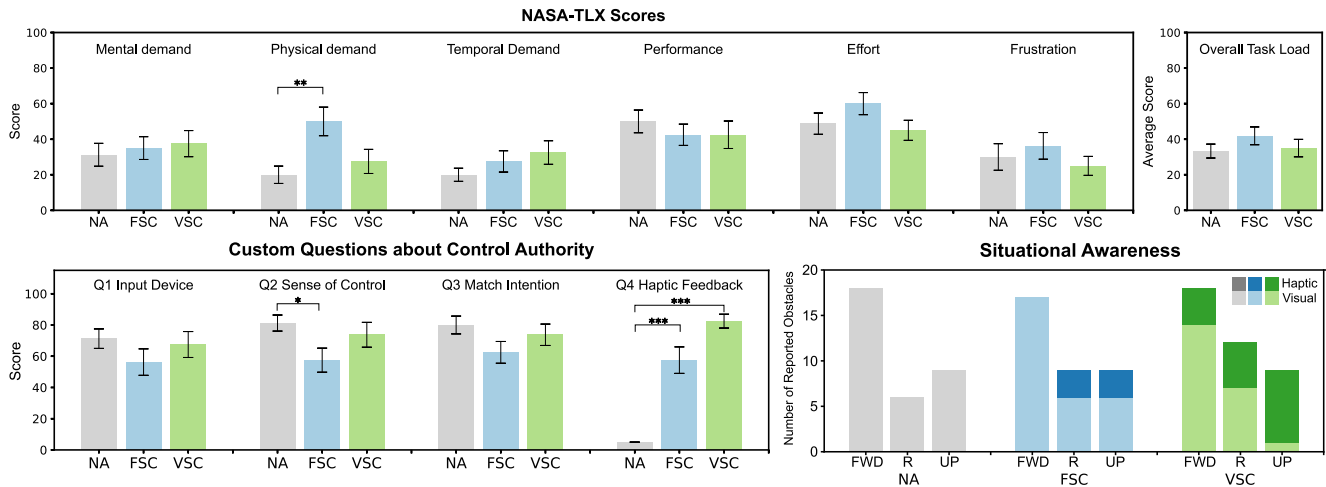


Fig. 8: Subjective measurements and situational awareness results grouped by feedback conditions (NA, FSC, VSC) and flying directions (forward, right, upward). The error bars represent the standard error of the mean (SEM),  $*p < 0.05$ ,  $**p < 0.01$ , and  $***p < 0.001$ .

steering forward, when the operator had a clear view of incoming obstacles. However, when the UAV was steering right or upward, visual information was limited so participants relied more on haptic feedback to steer the UAV. This suggested that future algorithms may dynamically adjust haptic feedback by assessing the visual capacity of UAVs during flight.

### C. Comparing Vibrotactile Feedback and Force Feedback

On-body vibrotactile feedback solved many of the limitations inherent in joystick-based haptic systems, e.g., oscillatory movement. In FSC, we noticed that participants struggled with the force feedback and often oversteered the UAV, resulting in oscillation behavior in the narrow tunnel (Figure 9). This observation was also confirmed by the total distance results, where FSC caused exceptionally long distances when flying to the right. In VSC, however, decoupling the input and output channels via the RC controller and AeroHaptix provided participants with full control authority over their UAV, thus eliminating oversteering.

Furthermore, our observations revealed distinct operation strategies. When using FSC, participants were passively engaged in the operation. They often exerted excessive control over the joystick (e.g., pushing it to the axis limit), and relied solely on the force feedback to maneuver UAVs and avoid obstacles. Collision avoidance came at the cost of control authority deprivation and low engagement. In contrast, VSC enhanced participants' awareness of obstacles without directly affecting control, promoting active engagement and thoughtful actions. When vibrotactile cues were present, participants would carefully reposition the UAV until they found a safe navigation path, as evidenced by the reduced input disagreement (Figure 7). Although VSC slightly raised mental workload, we believe the intuitive actuator layout would mitigate this during long-term usage.

## VIII. LIMITATIONS AND FUTURE WORK

Although the results showed that on-body vibrotactile feedback was effective at enhancing collision avoidance in

UAV teleoperation, there are also a few limitations. First, the upper-body vibrations have some limitations when representing downward obstacles. To compensate for these directions during the system evaluation, we mapped downward obstacles to the lower back actuators. In the future, extending vibrotactile feedback to the upper limbs or lower body could alleviate this problem.

Second, UAV teleoperation was simulated in a simplified virtual environment, without considering real-world complexities such as communication delays, inaccurate UAV state estimations, or control input constraints, as outlined by Lam [32]. To further validate vibrotactile feedback usage in real-world settings, we plan to integrate AeroHaptix into commercial UAVs using developer tools such as DJI SDKs.

Future work could leverage more vibration parameters to enrich obstacle information. Currently, we only modulated the actuator positions and vibration intensities to convey obstacle directions and risks. As prior research has suggested that frequency, spatial, and temporal patterns could also be viable for rendering spatial information [17], there is potential to represent complex information, such as obstacle types and mobility, during teleoperation tasks.

## IX. CONCLUSION

This work introduced AeroHaptix, a novel vibrotactile feedback system for collision avoidance during UAV teleoperation. The system was built using custom hardware that featured high-density actuators, fine-grained control, and low-latency communication. An optimal actuator layout was derived from a perceptual study to ensure obstacle directions could be uniformly conveyed across the upper body. Incorporated with a novel multi-point feedback algorithm MultiCBF, AeroHaptix enhanced collision avoidance, with reduced workload, increased situational awareness, and improved control authority. These findings suggested the potential for further haptic technology advancements in UAV teleoperation.



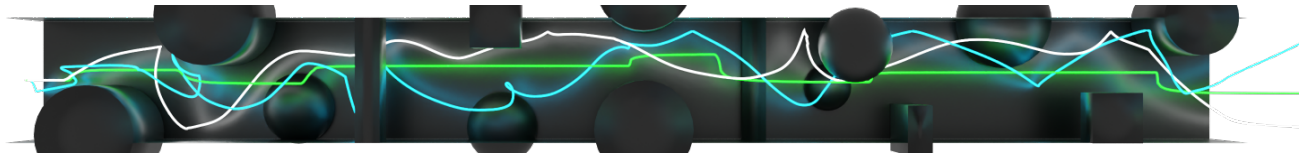


Fig. 9: Top-down view of sample trajectories from NA (white), FSC (blue), and VSC (green) conditions when flying to the right.

## REFERENCES

- [1] T. M. Lam, H. W. Boschloo, M. Mulder, and M. M. Van Paassen, "Artificial force field for haptic feedback in uav teleoperation," *IEEE Trans. on Syst., Man, and Cybern.-Part A: Syst. and Humans*, vol. 39, no. 6, pp. 1316–1330, 2009.
- [2] A. M. Brandt and M. B. Colton, "Haptic collision avoidance for a remotely operated quadrotor uav in indoor environments," in *2010 IEEE Int. Conf. on Syst., Man and Cybern.* IEEE, 2010, pp. 2724–2731.
- [3] X. Hou and R. Mahony, "Dynamic kinesthetic boundary for haptic teleoperation of vtol aerial robots in complex environments," *IEEE Trans. on Syst., Man and Cybern.: Syst.*, vol. 46, no. 5, pp. 694–705, 2015.
- [4] D. Zhang, G. Yang, and R. P. Khurshid, "Haptic teleoperation of uavs through control barrier functions," *IEEE Trans. on Haptics*, vol. 13, no. 1, pp. 109–115, 2020.
- [5] N. T. Inc, "Novint falcon," <https://hapticshouse.com/pages/novints-falcon-haptic-device>, 2024, accessed: Feb 24, 2024.
- [6] D. Syst., "Touch haptic device," <https://www.3dsystems.com/haptics-devices/touch>, 2024, accessed: Feb 24, 2024.
- [7] F. Dimension, "Force dimension - haptic devices," <https://www.forcedimension.com/products>, 2024, accessed: Feb 24, 2024.
- [8] D. Zhang, R. Tron, and R. P. Khurshid, "Haptic feedback improves human-robot agreement and user satisfaction in shared-autonomy teleoperation," in *2021 IEEE Int. Conf. on Robot. and Automat. (ICRA)*. IEEE, 2021, pp. 3306–3312.
- [9] R. M. Philbrick and M. B. Colton, "Effects of haptic and 3d audio feedback on operator performance and workload for quadrotor uavs in indoor environments," *J. of Robotics and Mechatronics*, vol. 26, no. 5, pp. 580–591, 2014.
- [10] A. M. Brandt, "Haptic collision avoidance for a remotely operated quadrotor uav in indoor environments," 2009.
- [11] V. Ho, C. Borst, M. M. van Paassen, and M. Mulder, "Increasing acceptance of haptic feedback in uav teleoperation by visualizing force fields," in *2018 IEEE Int. Conf. on Syst., Man, and Cybern. (SMC)*. IEEE, 2018, pp. 3027–3032.
- [12] S.-G. Hong, B. S. Kim, S. Kim, and J.-J. Lee, "Artificial force reflection control for teleoperated mobile robots," *Mechatronics*, vol. 8, no. 6, pp. 707–717, 1998.
- [13] H. W. Boschloo, T. M. Lam, M. Mulder, and M. Van Paassen, "Collision avoidance for a remotely-operated helicopter using haptic feedback," in *2004 IEEE Int. Conf. on Syst., Man and Cybern.*, vol. 1. IEEE, 2004, pp. 229–235.
- [14] X. Hou and R. Mahony, "Dynamic kinesthetic boundary for haptic teleoperation of aerial robotic vehicles," in *2013 IEEE/RSJ Int. Conf. on Intell. Robots and Syst.* IEEE, 2013, pp. 4549–4950.
- [15] H. Courtois, N. Aouf, K. Ahiska, and M. Cecotti, "Oast: Obstacle avoidance system for teleoperation of uavs," *IEEE Trans. on Human-Machine Syst.*, vol. 52, no. 2, pp. 157–168, 2022.
- [16] C. Louison, F. Ferlay, and D. R. Mestre, "Spatialized vibrotactile feedback contributes to goal-directed movements in cluttered virtual environments," in *2017 IEEE Symp. on 3D User Interfaces (3DUI)*. IEEE, 2017, pp. 99–102.
- [17] V. A. de Jesus Oliveira, L. Brayda, L. Nedel, and A. Maciel, "Designing a vibrotactile head-mounted display for spatial awareness in 3d spaces," *IEEE Trans. on Vis. and Comp. Graph.*, vol. 23, no. 4, pp. 1409–1417, 2017.
- [18] J. Y. F. Lee, N. Rajeev, and A. Bhojan, "Goldeye: Enhanced spatial awareness for the visually impaired using mixed reality and vibrotactile feedback," in *ACM Multimedia Asia*, 2021, pp. 1–7.
- [19] G. Flores, S. Kurniawan, R. Manduchi, E. Martinson, L. M. Morales, and E. A. Sisbot, "Vibrotactile guidance for wayfinding of blind walkers," *IEEE Trans. on Haptics*, vol. 8, no. 3, pp. 306–317, 2015.
- [20] H.-C. Wang, R. K. Katschmann, S. Teng, B. Araki, L. Giarré, and D. Rus, "Enabling independent navigation for visually impaired people through a wearable vision-based feedback system," in *2017 IEEE Int. Conf. on Robotics and Automat. (ICRA)*. IEEE, 2017, pp. 6533–6540.
- [21] M. A. B. Mohammed Zaffir and T. Wada, "Presentation of robot-intended handover position using vibrotactile interface during robot-to-human handover task," in *Proc. of the 2024 ACM/IEEE Int. Conf. on Human-Robot Interact.*, 2024, pp. 492–500.
- [22] S. Grushko, A. Vysocký, D. Heczko, and Z. Bobovský, "Intuitive spatial tactile feedback for better awareness about robot trajectory during human-robot collaboration," *Sensors*, vol. 21, no. 17, p. 5748, 2021.
- [23] P. Xia, K. McSweeney, F. Wen, Z. Song, M. Krieg, S. Li, X. Yu, K. Crippen, J. Adams, and E. J. Du, "Virtual telepresence for the future of rov teleoperations: opportunities and challenges," in *SNAME Offshore Symp.* SNAME, 2022, p. D011S001R001.
- [24] P. G. De Barros, R. W. Lindeman, and M. O. Ward, "Enhancing robot teleoperator situation awareness and performance using vibro-tactile and graphical feedback," in *2011 IEEE Symp. on 3D User Interfaces (3DUI)*. IEEE, 2011, pp. 47–54.
- [25] D. Wittchen, K. Spiel, B. Fruchard, D. Degraen, O. Schneider, G. Freitag, and P. Strohmeier, "Tactjam: An end-to-end prototyping suite for collaborative design of on-body vibrotactile feedback," in *16th Int. Conf. on Tangible, Embedded, and Embodied Interact.*, 2022, pp. 1–13.
- [26] A. Dementyev, P. Getreuer, D. Kanevsky, M. Slaney, and R. F. Lyon, "Vhp: vibrotactile haptics platform for on-body applications," in *The 34th Annu. ACM Symp. on User Interface Softw. and Technol.*, 2021, pp. 598–612.
- [27] bHaptics, "bhaptics: Tactile feedback for vr, gaming, and music," 2023. [Online]. Available: <https://www.bhaptics.com/>
- [28] J. B. Van Erp, "Presenting directions with a vibrotactile torso display," *Ergonomics*, vol. 48, no. 3, pp. 302–313, 2005.
- [29] H. Elsayed, M. Weigel, F. Müller, M. Schmitz, K. Marky, S. Günther, J. Riemann, and M. Mühlhäuser, "Vibromap: Understanding the spacing of vibrotactile actuators across the body," *Proceedings of the ACM on Interactive, Mobile, Wearable and Ubiquitous Technologies*, vol. 4, no. 4, pp. 1–16, 2020.
- [30] F. E. Van Beek, W. M. B. Tiest, and A. M. Kappers, "Anisotropy in the haptic perception of force direction and magnitude," *IEEE Trans. on Haptics*, vol. 6, no. 4, pp. 399–407, 2013.
- [31] H. Z. Tan, F. Barbagli, J. Salisbury, C. Ho, and C. Spence, "Force-direction discrimination is not influenced by reference force direction (short paper)," 2006.
- [32] T. M. Lam, M. Mulder, and M. Van Paassen, "Collision avoidance in uav tele-operation with time delay," in *2007 IEEE Int. Conf. on Syst., Man and Cybern.* IEEE, 2007, pp. 997–1002.
- [33] S. Omari, M.-D. Hua, G. Ducard, and T. Hamel, "Bilateral haptic teleoperation of vtol uavs," in *2013 IEEE Int. Conf. on Robot. and Automat.* IEEE, 2013, pp. 2393–2399.
- [34] S. Reyes, H. Romero, S. Salazar, R. Lozano, and O. Santos, "Outdoor haptic teleoperation of a hexarotor uav," in *2015 Int. Conf. on Unmanned Aircr. Syst. (ICUAS)*. IEEE, 2015, pp. 972–979.
- [35] S. Shah, D. Dey, C. Lovett, and A. Kapoor, "Airsim: High-fidelity visual and physical simulation for autonomous vehicles," in *Field and Service Robot.*, 2017. [Online]. Available: <https://arxiv.org/abs/1705.05065>
- [36] S. G. Hart and L. E. Staveland, "Development of nasa-tlx (task load index): Results of empirical and theoretical research," in *Advances in psychology*. Elsevier, 1988, vol. 52, pp. 139–183.
- [37] M. R. Endsley, "A systematic review and meta-analysis of direct objective measures of situation awareness: a comparison of sagat and spam," *Human factors*, vol. 63, no. 1, pp. 124–150, 2021.